

Microscopic analysis of ^{11}Li elastic scattering on protons and breakup processes within $^9\text{Li}+2n$ cluster model

V. K. Lukyanov,¹ D. N. Kadrev,² E. V. Zemlyanaya,¹ A. N. Antonov,²
K. V. Lukyanov,¹ M. K. Gaidarov,² and K. Spasova^{2,3}

¹*Joint Institute for Nuclear Research, Dubna 141980, Russia*

²*Institute for Nuclear Research and Nuclear Energy,
Bulgarian Academy of Sciences, Sofia 1784, Bulgaria*

³*University "Ep. K. Preslavski", Shumen 9712, Bulgaria*

In the paper, the results of analysis of elastic scattering and breakup processes in interactions of the ^{11}Li nucleus with protons are presented. The hybrid model of the microscopic optical potential (OP) is applied. This OP includes the single-folding real part, while its imaginary part is derived within the high-energy approximation (HEA) theory. For the $^{11}\text{Li}+p$ elastic scattering, the microscopic large-scale shell model (LSSM) density of ^{11}Li is used. The depths of the real and imaginary parts of OP are fitted to the elastic scattering data at 62, 68.4, and 75 MeV/nucleon, being simultaneously adjusted to reproduce the true energy dependence of the corresponding volume integrals. The role of the spin-orbit potential is studied and predictions for the total reaction cross sections are made. Also, the cluster model, in which ^{11}Li consists of $2n$ -halo and the ^9Li core having its own LSSM form of density, is adopted. The respective microscopic proton-cluster OP's are calculated and folded with the density probability of the relative motion of both clusters to get the whole $^{11}\text{Li}+p$ optical potential. The breakup cross sections of ^{11}Li at 62 MeV/nucleon and momentum distributions of the cluster fragments are calculated. An analysis of the single-particle density of ^{11}Li within the same cluster model accounting for the possible geometric forms of the halo-cluster density distribution is performed.

PACS numbers: 24.10.Ht, 25.40.Cm, 25.60.Gc, 21.10.Gv

I. INTRODUCTION

Recent experiments with radioactive ion beams have opened a new era in nuclear physics by providing the possibility to study the light nuclei far from stability. Indeed, the availability of the radioactive ion beams favored the discovery of halo nuclei [1]. A typical example is the neutron halo in the nucleus ^{11}Li , revealed as a consequence of its very large interaction radius, deduced from the measured interaction cross sections of ^{11}Li with various target nuclei [2–4]. The halo of the nucleus extends its matter distribution to a large radius. A hypothesis based on the early data [2] about the important role played by the neutron pairing for the stability of nuclei near the drip line is suggested in Refs. [5, 6] and, in particular, the direct link of the matter radius to the $2n$ weak binding in ^{11}Li is claimed to be attributed to its configuration as a ^9Li core coupled to a di-neutron.

The experiments that give evidences of the existence of a halo in this nucleus are related not only to measurements of the total reaction cross section for ^{11}Li projectiles but also to the momentum distributions of the ^9Li or neutron fragments following the breakup of ^{11}Li at high energies [7–10], e.g. the process $^{11}\text{Li}+^{12}\text{C}$ at $E = 800$ MeV/nucleon in Ref. [7]. Here we will mention also the experiments at lower energies $E = 60$ MeV/nucleon of scattering of ^{11}Li on ^9Be , ^{93}Nb and ^{181}Ta in [11] and of ^{11}Li on a wide range of nuclei from ^9Be to ^{238}U in [12]. It was shown that the momentum distribution of the breakup fragments has a narrow peak, much narrower than that observed in the fragmentation of well

bound nuclei. This property has been interpreted (e.g., [13–19]) to be related to the very large extension of the wave function, as compared to that of the core nucleus, leading to the existence of the nuclear halo. As pointed out in Ref. [17], the longitudinal component of the momentum (taken along the beam or z direction) gives the most accurate information on the intrinsic properties of the halo and is insensitive to details of the collision and the size of the target.

The differential cross sections for small-angle proton elastic scattering on Li isotopes at energies near 700 MeV/nucleon were measured in inverse kinematics with secondary nuclear beams at GSI (Darmstadt) [20]. They have been analyzed using the Glauber theory and information on the nuclear matter density distributions has been extracted. It was supposed that the two valence neutrons in ^{11}Li , which form the halo, could move in a wide region far from the ^9Li core that is related to the small two-neutron separation energy (~ 0.3 MeV).

The idea of existence of two-neutron halo in ^{11}Li was experimentally verified in measurements and studies of differential cross sections of the $^{11}\text{Li}+p$ elastic scattering in the energy range 60–75 MeV/nucleon [21–23]. The data analysis at 62 MeV/nucleon [21] showed that the adjusted phenomenological Woods-Saxon (WS) potential has a shallow real part and an imaginary part with a long tail. In Refs. [22, 23] the data at 65–75 MeV/nucleon were analyzed using the parameter free cluster-orbital shell-model approximation (COSMA) [24] and a conclusion was drawn that the $^{11}\text{Li}+p$ scattering is mainly determined by scattering on the ^9Li core. In various works

(e.g., Refs. [25–29]) the calculations of the $^{11}\text{Li}+p$ differential cross sections in the energy range $E < 100$ MeV/nucleon differ between themselves by the assumptions how the $^{11}\text{Li}+p$ optical potential to be constructed. Most of them use the simple folding approach to the real part of OP (ReOP) without accounting for the exchange terms and with introducing different forms of effective nucleon-nucleon (NN) interactions. To calculate the folding potentials, the constituent $^9\text{Li}+2n$ cluster model was usually employed, in which the ^{11}Li density has two separated parts taken in explicit forms. Various suggestions were made for the imaginary part of OP (ImOP) like WS and Gaussian forms or calculated within the t -matrix method. Then, the cross sections were computed numerically by using the eikonal approximation or starting with the Glauber multiple scattering theory. The more complicated model of ^{11}Li treated as a $^9\text{Li}+n+n$ three-body system was developed in Ref. [30], where the effects of the halo distribution in ^{11}Li in correspondence to different parts of the three-body wave function are manifested in the elastic cross section.

Generally, here we would like to outline the advantages of the microscopic analyses using the coordinate-space g -matrix folding method (e.g., Ref. [31]), as well as works (e.g., Ref. [32]), where the ReOP is microscopically calculated using effective NN interactions within a folding approach [33–36] and including also the exchange terms in it. In the recent works [37, 38] the $^{11}\text{Li}+p$ elastic scattering cross sections were analyzed using folding procedure and effective NN forces to calculate the real OP taking into account only its direct part but not the exchange one. In Ref. [37] the volume ImOP was taken either in a WS form or in the form of the direct folded ReOP and in Ref. [38] an application of the microscopic OP [39, 40] developed on the base of the HEA theory [41, 42] was also made. To this end phenomenological densities (Gaussian-types and COSMA) have been used in the calculations [37] and the LSSM densities of $^9,^{11}\text{Li}$ [43] in Ref. [38], as well.

The aims of our work can be presented as follows. First, we study elastic scattering cross section for $^{11}\text{Li}+p$ at three incident energies ($E < 100$ MeV/nucleon) using microscopically calculated OP's within the hybrid model [39]. The ReOP includes the direct and exchange terms and the ImOP is based on the HEA. We follow our previous works [44–46], where this model was applied to elastic scattering of exotic nuclei $^6,^8\text{He}$ with use of their LSSM densities, and thus avoiding an adjustment of free parameters. As in Ref. [45], we pay attention to the ambiguity problem when fitting the coefficients N 's that renormalize the strengths of different parts of OP. This ambiguity is minimized in Ref. [47] by testing the condition that the true energy dependence of the volume integrals must fulfill. Second, in addition to the analysis of elastic scattering cross sections, we estimate other characteristics of the reaction mechanism such as the ^{11}Li total reaction and breakup cross sections. The theoretical scheme used in this second part of the work is based on the pro-

cedure from the first part to calculate microscopically the potentials necessary for the evaluation of the other quantities within the model. The calculations are performed by using the $^{11}\text{Li}+p$ OP constructed as a sum of the microscopically calculated OP of $^9\text{Li}+p$ and the $(2n\text{-halo})+p$ potential folded with a density probability of the relative motion of clusters. For a more consistent description of the halo structure of ^{11}Li we calculate the fragment momentum distributions from $^{11}\text{Li}+p$ reaction at 62 MeV/nucleon within the same breakup reaction model and present predictions for them. Finally, we give results for the single-particle density distribution of ^{11}Li within the true two-cluster model considering the relative motion of clusters ($^9\text{Li}+h$) that is ensured by the respective wave function and make a comparison with other calculations.

The structure of this article is the following. The theoretical scheme to calculate microscopically the real and imaginary parts of the OP and the spin-orbit term, as well as the results of the calculations of the elastic scattering of ^{11}Li on protons and the discussion are given in Sec. II. The next Sec. III contains the basic expressions to estimate the ^{11}Li breakup and to calculate the momentum distributions of its products. The same Section contains the results of the total breakup cross sections, the momentum distributions of clusters and the single-particle density distribution of ^{11}Li calculated within the breakup model of ^{11}Li . The summary and conclusions of the work are given in Sec. IV.

II. ELASTIC SCATTERING OF ^{11}Li ON PROTONS AT $E < 100$ MEV/NUCLEON

A. Microscopic ReOP

The optical potential used in our calculations has the form

$$U_{opt} = V^F(r) + iW(r). \quad (1)$$

In Sec. IIC we add also a spin-orbit term to U_{opt} from Eq. (1).

The real part of the nucleon-nucleus OP is assumed to be a result of a folding of the nuclear density and of the effective NN potential and involves the direct and exchange parts (e.g., Refs. [33–35], see also [44, 45]):

$$V^F(r) = V^D(r) + V^{EX}(r). \quad (2)$$

The direct part $V^D(r)$ is composed by the isoscalar (IS) and isovector (IV) contributions:

$$V_{IS}^D(r) = \int \rho_2(\mathbf{r}_2)g(E)F(\rho_2)v_{00}^D(s)d\mathbf{r}_2, \quad (3)$$

$$V_{IV}^D(r) = \int \delta\rho_2(\mathbf{r}_2)g(E)F(\rho_2)v_{01}^D(s)d\mathbf{r}_2 \quad (4)$$

with $\mathbf{s} = \mathbf{r} + \mathbf{r}_2$, and

$$\rho_2(\mathbf{r}_2) = \rho_{2,p}(\mathbf{r}_{2,p}) + \rho_{2,n}(\mathbf{r}_{2,n}), \quad (5)$$

$$\delta\rho_2(\mathbf{r}_2) = \rho_{2,p}(\mathbf{r}_{2,p}) - \rho_{2,n}(\mathbf{r}_{2,n}). \quad (6)$$

In Eqs. (5) and (6) $\rho_{2,p}(\mathbf{r}_{2,p})$ and $\rho_{2,n}(\mathbf{r}_{2,n})$ are the proton and neutron densities of the target nucleus. The expressions for the energy and density dependence of the effective NN interaction (the formulae for $g(E)$ and $F(\rho)$) are given e.g., in Ref. [45]. For the NN potentials v_{00}^D and v_{01}^D we use the expression from Ref. [35] for the CDM3Y6 type of the effective interaction based on the Paris NN potential. The isoscalar part of the exchange contribution to the ReOP has the form:

$$V_{IS}^{EX}(r) = g(E) \int \rho_2(\mathbf{r}_2, \mathbf{r}_2 - \mathbf{s}) F(\rho_2(\mathbf{r}_2 - \mathbf{s}/2)) \times v_{00}^{EX}(s) j_0(k(r)s) d\mathbf{r}_2, \quad (7)$$

ρ_2 being the one-body density matrix. It is shown in Ref. [44] how the isovector part of the exchange ReOP can be obtained. Here we would like to emphasize the general importance of the account for the exchange part of the OP. As shown on different examples in Ref. [35], the exchange effects lead, for instance, to a particular energy dependence of the total potential, to different signs of the direct and exchange inelastic form factors and others, so they should be treated as accurately as possible.

The LSSM proton and neutron densities used in our work for ^{11}Li are calculated in a complex $2\hbar\omega$ shell-model space using the WS basis of single-particle wave functions with exponential asymptotic behavior [43], which is in principle the realistic one. Here we would like to discuss this point. In many works, to simplify the analytical studies and calculations one uses basic functions and densities with Gaussian asymptotics of the type $\exp(-ar^2)$, while it has to be exponential one $\exp(-br)/r$, where the parameter b is related to the bound energy of the particle in the upper shell. This difference can affect the results for the cross sections in the region of relatively large angles of scattering. This point was one of the reasons the LSSM densities [43] for $^{9,11}\text{Li}$ to be used in our work.

B. Optical potential within the high-energy approximation

In the present work we use the hybrid model of OP [39], in which its imaginary part was derived within the HEA theory [41, 42], while the real part is obtained as prescribed by the folding procedure from Sec. IIA. The cross sections are calculated by means of the DWUCK4 code [48] for solving the Schrödinger equation. To obtain

the HEA OP one can use the definition of the eikonal phase as an integral of the nucleon-nucleus potential over the trajectory of the straight-line propagation, and has to compare it with the corresponding Glauber expression for the phase in the optical limit approximation. In this way, the HEA OP is obtained as a folding of the form factors of the nuclear density and the NN amplitude $f_{NN}(q)$ [39, 40]:

$$U_{opt}^H = V^H + iW^H = -\frac{\hbar v}{(2\pi)^2} (\bar{\alpha}_{NN} + i) \bar{\sigma}_{NN} \times \int_0^\infty dq q^2 j_0(qr) \rho_2(q) f_{NN}(q). \quad (8)$$

In Eq. (8) $\bar{\sigma}_{NN}$ and $\bar{\alpha}_{NN}$ are, respectively, the NN total scattering cross section and the ratio of the real to imaginary part of the forward NN scattering amplitude, both averaged over the isospin of the nucleus. These two quantities have been parametrized in [49, 50] as functions of energies up to 1 GeV. The values of $\bar{\sigma}_{NN}$ and $\bar{\alpha}_{NN}$ can also account for the in-medium effect by a factor from Ref. [51].

C. The spin-orbit term

The expression for the spin-orbit contribution to the OP used in our work is added to the right-hand side of Eq. (1) and has the form:

$$V_{LS}(r) = 2\lambda_\pi^2 \left[V_0 \frac{1}{r} \frac{df_R(r)}{dr} + iW_0 \frac{1}{r} \frac{df_I(r)}{dr} \right] (\mathbf{1} \cdot \mathbf{s}), \quad (9)$$

where $\lambda_\pi^2 = 2 \text{ fm}^2$ is the squared pion Compton wavelength, V_0 and W_0 are the real and imaginary parts of the microscopic OP at $r=0$. In our work, in Eq. (9) the functions $f_R(r)$ and $f_I(r)$ are taken as WS forms $f(r, R_R, a_R)$ and $f(r, R_I, a_I)$ with the half-radius $R_R(R_I)$ and diffuseness $a_R(a_I)$ parameters obtained by the best fit of the WS potential to the microscopically calculated real $V(r)$ and imaginary $W(r)$ parts of the OP.

D. Results of calculations of $^{11}\text{Li}+p$ elastic scattering

In the beginning of this subsection we consider $^{11}\text{Li}+p$ elastic scattering at three energies, 62, 68.4, and 75 MeV/nucleon, for which the differential cross sections have been measured [21–23]. The respective folding optical potentials V^F and W^H are calculated by the procedure described in the previous subsections IIA.B.C. using Eqs. (1–9) and then, the whole OP is constructed in the form

$$U_{opt}(r) = N_R V^F(r) + iN_I W^H(r) + 2\lambda_\pi^2 \left\{ N_R^{SO} V_0^F \frac{1}{r} \frac{df_R(r)}{dr} + iN_I^{SO} W_0^H \frac{1}{r} \frac{df_I(r)}{dr} \right\} (\mathbf{1} \cdot \mathbf{s}). \quad (10)$$

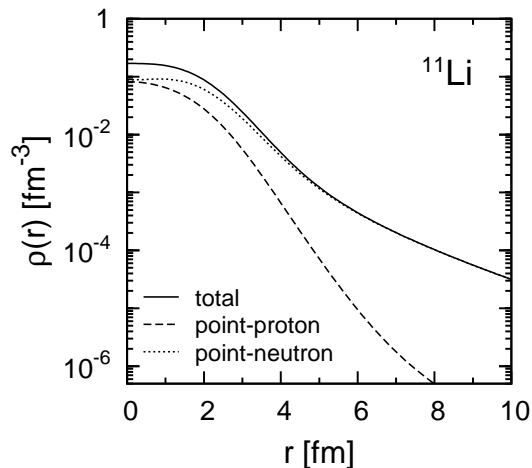


FIG. 1. Total (normalized to $A = 11$), point-proton (normalized to $Z = 3$) and point-neutron (normalized to $N = 8$) densities of ^{11}Li obtained in the LSSM approach [43].

The OP $U_{opt}(r)$ (10) is applied to calculate the elastic scattering differential cross sections using the program DWUCK4 [48]. The number of partial waves is controlled by the parameter LMAX that corresponds to the maximum partial wave for the distorted waves. We use the parameter LMAX=100. For the densities of protons and neutrons of ^{11}Li we use the LSSM ones [43] (shown in Fig. 1) that have an exponential asymptotics which is the correct one. As can be seen from Eq. (10), we introduce and consider the set of N coefficients as parameters that can be found by fitting the calculated to the experimental differential cross sections of the $^{11}\text{Li}+p$ elastic scattering. Moreover, the fitting procedure can be constrained by additional conditions on the behavior of the OP's (as in Refs. [44–46] and will be seen below). The real and imaginary parts of the SO optical potential in (10) are approximated by Woods-Saxon form. Their parameters $V_0^F(W_0^H)$, $R_R(R_I)$ and $a_R(a_I)$ were obtained by a fitting procedure to the respective calculated microscopic potentials $V^F(r)$ and $W^H(r)$. We take the ImOP in two forms, the microscopically obtained W^H within HEA ($W = W^H$) or the form of the folded real potential V^F ($W = V^F$).

Concerning our approach using the set of N coefficients as parameters we consider it as the appropriate physical basis, which constrains the fitting procedure by the established model forms of the potentials. We emphasize that in our work we do not aim to find perfect agreement with the experimental data. In this sense, however, the usage of the fitting parameters (N 's) related to the depths of the different components of the OP's can be considered as a way to introduce a quantitative measure of the deviations of the predictions of our method (with the account for the exchange contributions to OP) from the reality (e.g., the differences of N 's from unity for given energies, as can be seen below). Thus, the closeness of the N 's values to unity could show the ability of

TABLE I. Values of the N 's parameters, χ^2 and σ_R (in mb) in the case of $^{11}\text{Li}+p$ at 62 MeV/nucleon for the results shown in Fig. 3.

W	N_R	N_I	N_R^{SO}	N_I^{SO}	χ^2	σ_R
W^H	0.871	0.953			1.415	456.97
	0.870	0.965			1.435	459.37
	0.873	0.948			1.423	455.98
	0.854	0.974	0.028	0.000	1.468	461.21
V^F	0.953	0.448			5.567	389.72
	0.956	0.398			5.726	361.02
	0.670	0.251	0.338	0.000	5.027	258.65
	0.623	0.266	0.402	0.000	5.538	270.05

the approach to give the absolute values of the intensity of the OP's.

The microscopic real part (V^F) of OP and HEA imaginary part (W^H) calculated using LSSM densities of ^{11}Li are shown in Fig. 2 for different energies. In Fig. 3 we give as an example the differential cross section of the elastic scattering $^{11}\text{Li}+p$ at 62 MeV/nucleon in the cases when $W = W^H$ and $W = V^F$ with and without accounting for the spin-orbit term in Eq. (10). The renormalization parameters N are determined by a fitting procedure. The results of the calculations are close to each other and that is why all of them are presented inside areas shown in Fig. 3. The following definition of χ^2 is used:

$$\chi^2 = \frac{1}{N} \sum_{i=1}^N \left[\frac{\sigma^{\text{exp}}(\vartheta_i) - \sigma^{\text{th}}(\vartheta_i)}{\Delta\sigma^{\text{exp}}(\vartheta_i)} \right]^2, \quad (11)$$

where $\sigma^{\text{th}}(\vartheta_i)$ and $\sigma^{\text{exp}}(\vartheta_i)$ are the theoretical and experimental values of the differential cross sections ($d\sigma/d\Omega$), and $\Delta\sigma^{\text{exp}}(\vartheta_i)$ is the experimental error. The blue area in Fig. 3 includes four curves corresponding to $W = W^H$ (from which three curves obtained without SO term and one with the SO term), while the grey one includes four curves corresponding to $W = V^F$ (from which two curves obtained without SO term and two curves with the SO term). We give in Table I the values of the N 's parameters, χ^2 and the total reaction cross sections σ_R .

It can be seen from Fig. 3 the satisfactory overall agreement of both areas of curves with the experimental data. However, we note the better agreement in the case when $W = W^H$ (the blue area) and the values of χ^2 are between 1.40 and 1.47, while in the case $W = V^F$ they are between 5.00 and 5.80. The situation is similar also for the other energies. So, in our further calculations we use only ImOP $W = W^H$. Second, we note that the values of σ_R are quite different in both cases ($\sigma_R \approx 455\text{--}462$ mb for $W = W^H$ and $\sigma_R \approx 260\text{--}390$ mb for $W = V^F$). Third, one can see from Table I and from the comparison with the data in Fig. 3 that the role of the SO term is weak. Its effects turn out to be to decrease the values of

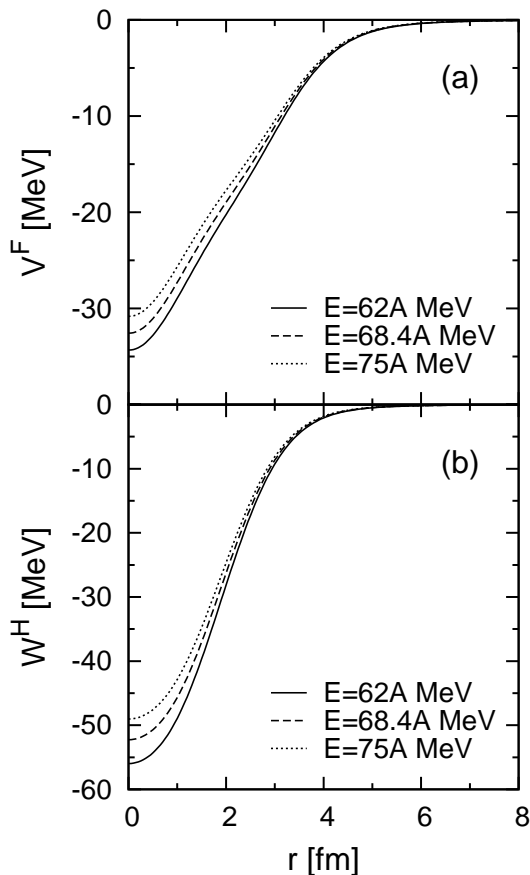


FIG. 2. Microscopic real part (V^F) of OP (a) and HEA imaginary part (W^H) (b) calculated using the LSSM densities for energies $E = 62$ (solid lines), 68.4 (dashed lines) and 75 MeV/nucleon (dotted lines).

N_R and to increase the values of N_R^{SO} (see the last two lines in Table I).

As is known, the problem of the ambiguity of the parameters N arises when the fitting procedure is applied to a limited number of experimental data (see, e.g., the calculations and discussion in our previous works [44–46]). Due to the fact that the fitting procedure belongs to the class of the ill-posed problems (see, e.g., Ref. [52]), it becomes necessary to impose some physical constraints on the choice of the set of parameters N . The total cross section of scattering and reaction is one of them, however, the corresponding experimental values are missing at the energy interval considered in the present work.

Another physical criterion that has to be imposed on the choice of the N values is the behavior of the volume integrals

$$J_V = \frac{4\pi}{A} \int dr r^2 [N_R V^F(r)], \quad (12)$$

$$J_W = \frac{4\pi}{A} \int dr r^2 [N_I W^H(r)] \quad (13)$$

as functions of the energy.

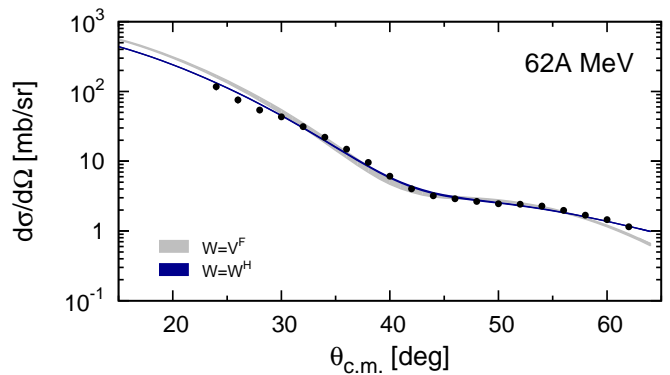


FIG. 3. (Color online) The $^{11}\text{Li}+p$ elastic scattering cross section at $E = 62$ MeV/nucleon using U_{opt} [Eq. (10)] for values of the parameters shown in Table I. Dark (blue) area: $W = W^H$, pale (grey) area: $W = V^F$. The experimental data are taken from Ref. [21].

We show in Fig. 4 the results of our calculations of the $^{11}\text{Li}+p$ elastic scattering cross sections for the three energies $E = 62, 68.4$ and 75 MeV/nucleon. For each energy we present two curves, with and without accounting for the SO term. The corresponding values of the N 's parameters together with those of J_V , J_W , χ^2 and σ_R are given in Table II. In Fig. 5 we give the curves for the volume integrals J_V and J_W connecting the results obtained in our calculations with N 's values. We present them as better ones because first, the values of χ^2 are around unity, and second, there is a good agreement with the data including those of $\theta_{c.m.}$ up to 60° for 62 MeV/nucleon. One can see that the values of J_V are decreasing with the increase of the incident energy (with a small exception at 68.4 MeV/nucleon) that is in general agreement with the results from Ref. [53]. This is not the case for J_W , where its value for $E = 62$ MeV/nucleon is larger than for the others. Indeed, it was pointed out in [53] that the general behavior of the volume integral J_V is decreasing with the increase of the energy in the interval $0 < E < 100$ MeV/nucleon, while J_W increases with the increase of comparatively small energy and becomes almost constant at a larger energy. However, the same situation had appeared in the analysis of the same data at three energies within the semi-microscopic approach in Ref. [37], where the ReOP was calculated using a single-folding procedure with Gaussian, Gaussian-oscillator and COSMA forms of the single-particle density and the ImOP was taken phenomenologically in a Woods-Saxon form or equal to the form of the folded ReOP. In Fig. 6(a) are shown the curves of J_V corresponding to its values obtained in [37] for the cases of the four densities used. In addition, we show in Fig. 6(b) the values of J_W calculated using the corresponding fitted imaginary part of the OP's taken in a phenomenological WS form. One can see that the J_V has a reasonable behavior in agreement with the results from Ref. [53], while the values of J_W are in contradiction with them. Thus,

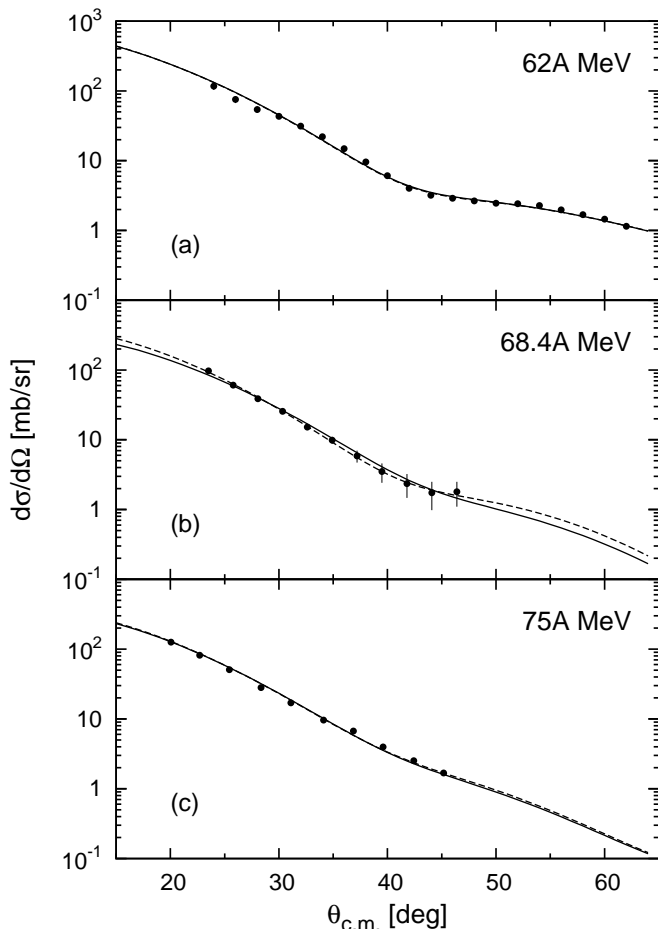


FIG. 4. The $^{11}\text{Li}+p$ elastic scattering cross section at $E = 62$, 68.4, and 75 MeV/nucleon. Solid line: without SO term; dashed line: with SO term. The values of N 's are given in Table II. The experimental data are taken from [21] for 62 MeV/nucleon, [22] for 68.4 MeV/nucleon, and [23] for 75 MeV/nucleon.

the problem arising in our work had appeared also in the semi-phenomenological approach in Ref. [37], in which a larger number of parameters has been used. A possible reason for such a behavior of J_W at this energy could be the change of the scattering mechanism with the increase of the angle of scattering when the other channels except the elastic one should be taken into consideration. Such a "strong" channel with its influence on the elastic one could be that of the fragmentation of ^{11}Li into clusters.

As a next step, we perform a methodical study of $^{11}\text{Li}+p$ elastic scattering cross section for $E = 62$ MeV/nucleon limiting our fitting procedure for the N 's parameters up to the experimental points for $\theta_{c.m.} \leq 46^\circ$. The result of this study is presented in Fig. 7. Doing so we consider now the experimental data for all three energies 62, 68.4, and 75 MeV/nucleon being at the same region of angles. The fit to this amount of data at 62 MeV/nucleon yields the new set of parameters: $N_R = 0.656$, $N_I = 0.164$ with $\chi^2 = 0.788$ and

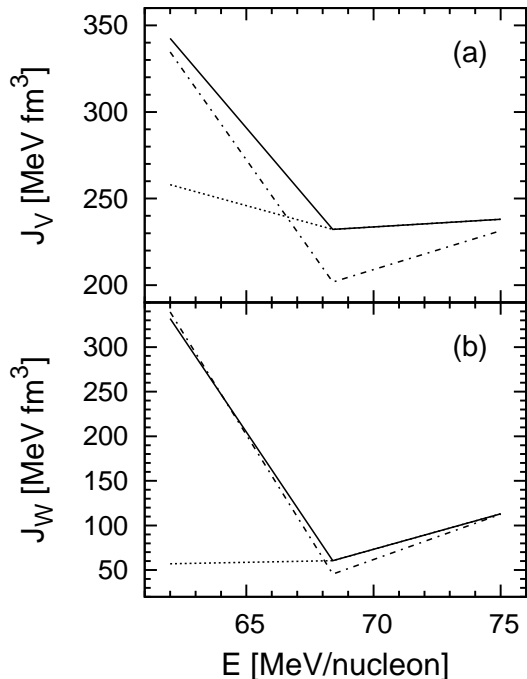


FIG. 5. The values of the volume integrals J_V and J_W [Eqs. (12) and (13)] as functions of the energy per nucleon for $^{11}\text{Li}+p$ elastic scattering. The N 's values are given in Table II. Solid line: without SO term of U_{opt} [Eq. (10)]; dash-dotted line: with SO term of U_{opt} . The additional values of J_V and J_W at $E = 62$ MeV/nucleon (connected by a dotted line with the other curves) are obtained in the case when the fitting procedure for the N 's parameters is limited up to the experimental points for $\theta_{c.m.} \leq 46^\circ$ (see the text).

$\sigma_R = 154.86$ mb. Now we obtain values of the volume integrals (without SO term of U_{opt}) $J_V = 257.973$ MeV fm^3 and $J_W = 57.136$ MeV fm^3 (shown in Fig. 5), while the obtained before values are $J_V = 342.47$ MeV fm^3 and $J_W = 332.015$ MeV fm^3 (see the first line in Table II). As a result, we get the behavior of J_V and J_W in a reasonable agreement with the conclusions of Ref. [53]. In our opinion, the procedure described above points out the role of the data at $\theta_{c.m.} > 46^\circ$ on the values of χ^2 and on the conclusions on the mechanism of the elastic scattering process.

III. BREAKUP PROCESSES WITHIN $^9\text{Li}+2n$ CLUSTER MODEL

A. Two-cluster model and applications

In this Section, in addition to the analysis of $^{11}\text{Li}+p$ elastic scattering cross section in Sec. II, we study other characteristics of the reaction mechanism, such as the ^{11}Li total reaction cross section, the breakup cross section and related quantities. This part of the work is based on the procedure for microscopic calculations of OP's presented in Sec. II. We consider a simple two-cluster model

TABLE II. Values of the N 's parameters, volume integrals J_V and J_W (in MeV fm^3), χ^2 and total reaction cross section σ_R (in mb) for results at three energies E (in MeV/nucleon) considered and shown in Fig. 4.

E	N_R	N_I	N_R^{SO}	N_I^{SO}	J_V	J_W	χ^2	σ_R
62	0.871	0.953			342.474	332.015	1.415	456.97
	0.851	0.974	0.028	0.000	334.610	339.332	1.468	461.21
68.4	0.625	0.186			232.210	60.489	1.328	153.44
	0.543	0.140	0.201	0.000	201.744	45.530	0.316	122.25
75	0.679	0.370			238.048	112.913		232.62
	0.660	0.369	0.045	0.000	231.387	112.607		232.62

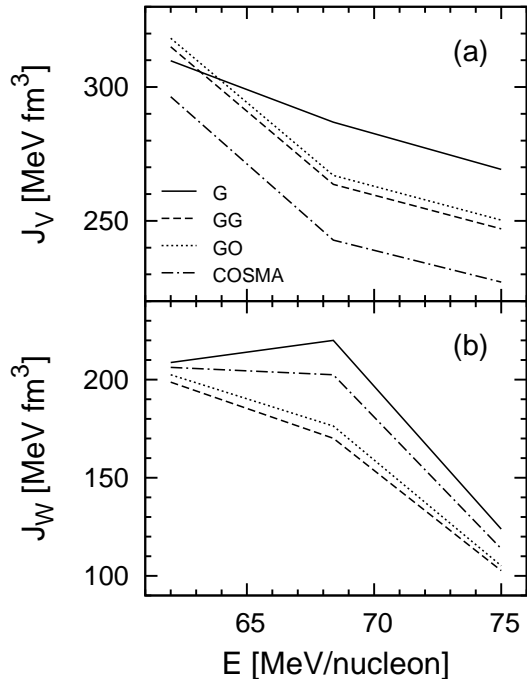


FIG. 6. The energy dependence of the volume integrals: (a) J_V obtained in [37] for folding potentials ReOP (V) calculated using two types of Gaussians (G and GG), Gaussian oscillator (GO) and COSMA densities of ^{11}Li for $^{11}\text{Li}+p$ elastic scattering; (b) J_W calculated using the fitted imaginary WS potentials corresponding to those real parts of OP that give J_V 's in (a).

that has been already used for ^6He for studying its elastic scattering and breakup reactions on nuclear targets [54]. Within this model for the ^{11}Li nucleus, first, the density distributions of ^9Li core (c -cluster) and $h = 2n$ -halo must be given. Second, the folding potentials of interaction of each of the clusters with the incident proton have to be computed. Then, the sum of these two potentials must be folded with the respective two-cluster density distribution of ^{11}Li that causes the necessity the wave function of the relative motion of two clusters to be known. We calculate the latter as a solution of the Schrödinger wave equation by using of WS potential and

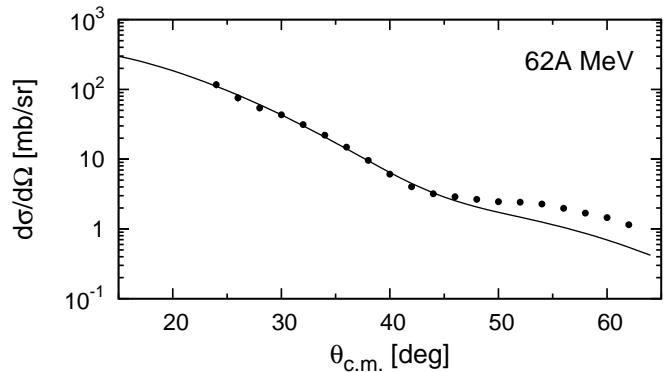


FIG. 7. The $^{11}\text{Li}+p$ elastic scattering cross section at $E = 62$ MeV/nucleon when the fitting procedure for the N 's parameters is limited only up to the experimental points for $\theta_{c.m.} \leq 46^\circ$. The obtained values of N_R , N_I , J_V , J_W , χ^2 , and σ_R are given in the text.

given $0s$ or $1s$ state for particle with reduced mass of both clusters. The WS parameters are obtained by fitting the energy of a given state to the empirical separation energy value of h -cluster $\varepsilon = 0.247$ MeV and the rms radius of the cluster function. For the latter we choose the value of 4.93 fm that is somehow "in between" the values obtained within the three-body COSMA [55] and deduced from shell-model calculations [56, 57]. Such two-cluster model takes an interspace between the two classes of approaches. In one of them each of the clusters has its own phenomenological density that is often used to fit the elastic scattering data. The second class includes microscopic three-body models using to a different extent the shell-model picture. Among them we would like to note COSMA (see, for example, Refs. [58, 59]), which has already successfully described a great amount of experimental data applying the Glauber scattering theory. Justifying our more simple two-cluster model, we hope, however, to keep the basic physical consideration avoiding some simplifications like folding without exchange effects, use of Gaussian-type functions for densities of clusters and bound-state wave functions of relative motion, use of phenomenological ImOP etc. We will always take into account the contribution of the exchange effects and

the wave function of the relative motion of two clusters is calculated for the fitted finite-range potential that has an exponential behavior. The bound-state two-cluster system requires a particular consideration. In the earlier works estimations were made using the wave function of $0s$ -state ($n=0$) of the ($c+h$) system, which does not have nodes inside the potential (except at $r=0$). However, it has been shown in Refs. [55, 57] that due to the violation of Pauli principle (Pauli-blocking effect in ^{11}Li ground state) the $1s$ - and $0p$ -states give the main contribution to the wave function of the two-cluster system with almost equal probabilities thus oscillating once inside the potential. Nevertheless, we will consider both $0s$ - and $1s$ -densities $\rho_0^{(0)}$ and $\rho_0^{(1)}$ in the further calculations and comparisons of the results.

In the present study, the interaction between the clusters is taken to be a WS potential with the adjusted geometrical parameters $R=1.0$ fm, $a=0.25$ fm and the

depth $V_0 = 32.55$ MeV for $0s$ -state and $R = 6.25$ fm, $a = 0.25$ fm, and $V_0 = 11.55$ MeV for $1s$ -state.

The s -state ($l=0$) wave function of the relative motion of two clusters is

$$\phi_{00}^{(n)}(\mathbf{s}) = \phi_0^{(n)}(s) \frac{1}{\sqrt{4\pi}}, \quad n=0,1 \quad (14)$$

and thus, the respective density distribution is defined as a probability for clusters to be at a mutual distance s :

$$\rho_0^{(n)}(\mathbf{s}) = |\phi_{00}^{(n)}(\mathbf{s})|^2 = \frac{1}{4\pi} |\phi_0^{(n)}(s)|^2. \quad (15)$$

In the framework of the $^9\text{Li}+2n$ model of ^{11}Li one can estimate the $^{11}\text{Li}+p$ OP as a sum of two OP's of interactions of the c - and h -clusters with protons folded with the density $\rho_0^{(n)}(s)$ ($n=0, 1$):

$$U^{(b,n)}(r) = V^{(b,n)} + iW^{(b,n)} = \int ds \rho_0^{(n)}(s) \left[U_c^{(n)}(\mathbf{r} + (2/11)\mathbf{s}) + U_h^{(n)}(\mathbf{r} - (9/11)\mathbf{s}) \right] = 2\pi \int_0^\infty \rho_0^{(n)}(s) s^2 ds \\ \times \int_{-1}^1 dx \left[U_c^{(n)}\left(\sqrt{r^2 + (2s/11)^2 + r(4/11)sx}\right) + U_h^{(n)}\left(\sqrt{r^2 + (9s/11)^2 - r(18/11)sx}\right) \right]. \quad (16)$$

In Eq. (16) $\mathbf{r} - (9/11)\mathbf{s} \equiv \mathbf{r}_h$ and $\mathbf{r} + (2/11)\mathbf{s} \equiv \mathbf{r}_c$ define the corresponding distances between the centers of each of the clusters and the arbitrary position of the nucleon in ^{11}Li nucleus, and $\mathbf{s} = \mathbf{s}_1 + \mathbf{s}_2 = (9/11)\mathbf{s} + (2/11)\mathbf{s}$ determines the relative distance between the centers of the two clusters, s_1 and s_2 being distances between the centers of ^{11}Li and each of the clusters, respectively. The potential $U_c^{(n)}$ in Eq. (16) is calculated within the microscopic hybrid model of OP described in Sect.IIA and B. For OP of the h - p interaction we use the sum of two v_{np} potentials as

$$U_h^{(n)} = 2v_{np} = 2v(r)(1 + i\gamma). \quad (17)$$

Such n - p complex potential has been used in the four-body model [25] in calculations of the $^{11}\text{Li}+p$ elastic scattering and it was shown that the cross sections are rather

insensitive to a precise form of the n - p potential taken in the form [60] (in MeV):

$$v(r) = 120e^{-1.487r^2} - 53.4e^{-0.639r^2} - 27.55e^{-0.465r^2} \quad (18)$$

with $\gamma = 0.4$.

We also intend to adopt the two-cluster model to calculate breakup reactions of ^{11}Li in collisions with the proton target. To this end the HEA method which has been developed in Refs. [15, 16] and applied in [54] for $^6\text{He}+^{12}\text{C}$ reaction will be used in the present study. For simplicity, further the superscript index ($n=0, 1$) which corresponds to the number of nodes of the relative-motion s -wave function of the two clusters will be omitted. To show briefly the eikonal formalism, we start with the probability that after the collision with a proton ($z \rightarrow \infty$) the cluster h or c with an impact parameter b remains in the elastic channel:

$$|S_i(b)|^2 = \exp \left[-\frac{2}{\hbar v} \int_{-\infty}^{\infty} dz W_i \left(\sqrt{b^2 + z^2} \right) \right], \quad i = c, h, \quad (19)$$

where W is the imaginary part of the microscopic OP (16). Consequently, the probability for the cluster to be removed from the elastic channel is $(1 - |S|^2)$. Thus, the common probability of both h and c clusters to

leave the elastic channel of the $^{11}\text{Li}+p$ scattering is $(1 - |S_h|^2)(1 - |S_c|^2)$. After averaging the latter by $\rho_0(s)$ (which characterizes the probability of h and c to be at a relative distance s), the total absorption cross section

is obtained:

$$\sigma_{abs}^{tot} = 2\pi \int_0^\infty b_h db_h [1 - |S_h(b_h)|^2][1 - I_c(b_h)], \quad (20)$$

where

$$I_c(b_h) = \int ds \rho_0(s) |S_c(b_c)|^2. \quad (21)$$

In Eq. (21)

$$b_c = \sqrt{s^2 \sin^2 \theta + b_h^2 + 2sb_h \sin \theta \cos(\varphi - \varphi_h)} \quad (22)$$

and it comes out from the relation $\mathbf{b}_c = \mathbf{b}_h + \mathbf{b}$ with $b = s \sin \theta$ being the projection of \mathbf{s} on the plane normal to the z -axis along the straight line trajectory of the incident nucleus.

In the case of a stripping reaction with removing h -cluster from ^{11}Li to the proton target, one should use the probability of h to leave the elastic channel $[1 - |S_h(b_h)|^2]$, and for c to continue its elastic scattering with a probability $|S_c(b_c)|^2$. Then the probability of the whole process is $|S_c(b_c)|^2 [1 - |S_h(b_h)|^2]$, and to get the total stripping cross section one has to average over $\rho_0(s)$ [see Eqs. (20) and (21)]. Similarly, the ^9Li transfer can be constructed, and the net contribution of both removal reactions yields the total breakup cross section:

$$\sigma_{bu}^{tot} = 2\pi \int_0^\infty b_h db_h \{ |S_h(b_h)|^2 + [1 - 2|S_h(b_h)|^2] I_c(b_h) \}. \quad (23)$$

The sum of both absorption [Eqs. (20) and (21)] and breakup [Eq. (23)] cross sections gives the total reaction

cross section:

$$\sigma_R^{tot} = 2\pi \int_0^\infty b_h db_h [1 - |S_h(b_h)|^2 I_c(b_h)]. \quad (24)$$

B. Momentum distributions of fragments

As is known (see, e.g., [15]), the differential and total cross sections (for elastic scattering, as well as for diffractive breakup and absorption) all require calculations of the probability functions of the \mathbf{k} -momentum distribution of a cluster in the two-cluster system $d^3P(\mathbf{b}, \mathbf{k})/d\mathbf{k}$ that depend on the impact parameter \mathbf{b} . The general expression for the probability functions can be written as [15]:

$$\frac{d^3P_\Omega(\mathbf{b}, \mathbf{k})}{d\mathbf{k}} = \frac{1}{(2\pi)^3} \left| \int ds \phi_{\mathbf{k}}^*(\mathbf{s}) \Omega(\mathbf{b}, \mathbf{r}_\perp) \phi_{00}^{(n)}(\mathbf{s}) \right|^2, \quad (25)$$

where $\Omega(\mathbf{b}, \mathbf{r}_\perp)$ is expressed by means of the two profile functions S_c and S_h [Eq. (19)] of the core and the di-neutron clusters, respectively. In Eq. (25) $\phi_{\mathbf{k}}(\mathbf{s})$ is the continuum wave function and \mathbf{k} is the relative momentum of both clusters in their center-of-mass frame. The vector \mathbf{r}_\perp is the projection of the relative coordinate \mathbf{s} between the centers of the two clusters on the plane normal to the z -axis mentioned above. The ground-state wave function of the relative motion of the two clusters ϕ_{00} is given for the s -state by Eq. (14). For calculations of e.g., the diffractive cross sections, the continuum wave function $\phi_{\mathbf{k}}$ is expanded in partial wave representation. If in this case the distortion in the final channel is neglected, the wave function $\phi_{\mathbf{k}}(\mathbf{s})$ is replaced by a plane wave. Then, following Ref. [15] for the s -state ($l = 0$) the expression for $d^2P_\Omega(\mathbf{b}, \mathbf{k})/dk_L dk_\perp$ will take the form:

$$\frac{d^2P_\Omega(\mathbf{b}, \mathbf{k})}{dk_L dk_\perp} = \frac{k_\perp}{16\pi^3 k^2} \left| \int ds \int d(\cos \theta_s) g(s) \sin(k s) \int d\varphi_s \Omega(\mathbf{b}, \mathbf{r}_\perp) \right|^2 \quad (26)$$

with

$$\Omega(\mathbf{b}, \mathbf{r}_\perp) = S_c(\mathbf{b}_c) S_h(\mathbf{b}_h). \quad (27)$$

In Eq. (26) $g(s) = r \phi_0^{(n)}(s) = r \sqrt{4\pi \rho_0^{(n)}(s)}$, where $\phi_0^{(n)}$ and $\rho_0^{(n)}$ are given in Eqs. (14) and (15). Hence, the

diffractive breakup cross section has the form

$$\left(\frac{d\sigma}{dk_L} \right)_{diff} = \int_0^\infty b_h db_h \int_0^{2\pi} d\varphi_h \int_0^\infty dk_\perp \frac{d^2P_\Omega(\mathbf{k}, \mathbf{b})}{dk_L dk_\perp} \quad (28)$$

with $d^2P_\Omega(\mathbf{b}, \mathbf{k})/dk_L dk_\perp$ from Eq. (26). The integrations over b_h and φ_h in Eq. (28) mean integration over the

impact parameter \mathbf{b}_h of the cluster h with respect to the

target.

$$\left(\frac{d\sigma}{dk_L}\right)_{str} = \frac{1}{2\pi^2} \int_0^\infty b_h db_h d\varphi_h [1 - |S_h(b_h)|^2] \int \rho d\rho d\varphi_\rho |S_c(b_c)|^2 \left[\int_0^\infty dz \cos(k_L z) \phi_0 \left(\sqrt{\rho^2 + z^2} \right) \right]^2. \quad (29)$$

Eq. (29) is obtained when the incident nucleus has spin equal to zero and for the s -state of the relative motion of both clusters in the nucleus expressed by Eq. (14) with $\mathbf{s} = \mathbf{r}_c - \mathbf{r}_h$, $\rho = \mathbf{b}_c - \mathbf{b}_h$, $\mathbf{s} = \rho + \mathbf{z}$ and b_c from Eq. (22).

C. Results of calculations for breakup processes

To estimate the ^{11}Li breakup on a proton target, we use the two-cluster model described in Sec. IIIA. As presented there, we intend to study some observables when the ^{11}Li nucleus with the $h = 2n$ -cluster separation energy of 0.247 MeV is considered as a system in the $l = 0$ state with principal quantum numbers $n = 0$ or $n = 1$. The respective WS potentials $V(s)$ and probabilities $\rho_0^{(n)}(s)$ [Eq. (15)] for the distance s between the clusters in ^{11}Li are shown for both $n = 0, 1$ in Fig. 8(a) and (b), respectively. It can be seen from Fig. 8(a) that the WS potential for $n = 0$ is about 2.8 times deeper than the one for the case of $n = 1$, although the shapes of both potentials are similar. We note also that the half radius of the $n = 1$ potential is equal to 6.25 fm and it is much larger than that of 1.01 fm of the $n = 0$ potential. Fig. 8(b) shows that the two densities differ from each other. Particularly, a steep drop of $n=1$ density is observed at $s \approx 3.8$ fm. Moreover, bearing in mind the results of fitting procedures in phenomenological potentials (e.g., in Ref. [20]) giving rms radius of about $5 \div 6$ fm for the constituent h -cluster density $\rho_h(r)$, we may conclude that in our consideration the $n = 1$ cluster state of ^{11}Li becomes preferable. On the other hand, the existence of long tails of $\rho_0^{(n=0,1)}(s)$ for both states provokes interest to test their effects in the further considerations.

Our next step is to apply the optical potential $U^{(b,n)}$ [Eq. (16)] constructed in the framework of the two-cluster model of ^{11}Li to calculate the differential cross section of the elastic scattering $^{11}\text{Li}+p$ at 62 MeV/nucleon. For the real part $V^{(b,n)}$ of this OP we use a single-folding procedure in which the LSSM density [43] is taken for the ^9Li cluster. The imaginary part $W^{(b,n)}$ of the OP is considered like before to be either $W = W^H$ or $W = V^F$. The calculated cross sections are shown in Fig. 9 and compared with the experimental data [21]. For both cases we give in Table III the values of the fitted renormalization coefficients N 's and the respective total cross sections for $n = 0$ and $n = 1$ cases. One can see from Fig. 9 that the angular distributions for both kinds of ImOP are closely

In the case of the stripping reaction when the h -cluster leaves the elastic channel it can be shown (following [15]) that the cross section takes the form:

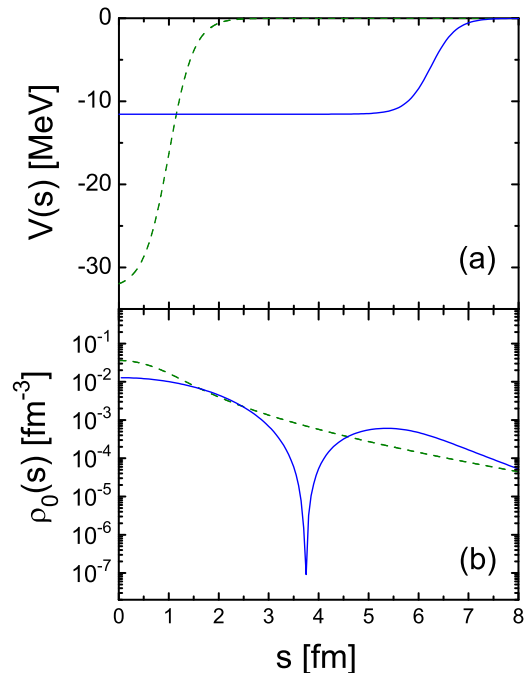


FIG. 8. (Color online) The WS potential $V(s)$ of the interaction between c and h clusters (a) and the two-cluster density distribution $\rho_0(s)$ normalized to unity (b) for the cases of $n=0$ (green dashed line) and $n=1$ (blue solid line).

displayed and they lead to a fairly good agreement with the experimental data. However, we note that the data are reproduced better again when $W = W^H$ for both $n=0, 1$ cases, as it was pointed out from the discussion of the results presented in Fig. 3 and obtained with the usage of the LSSM density for ^{11}Li .

In Table III the values of the total absorption σ_{abs}^{tot} , breakup σ_{bu}^{tot} and total reaction σ_R^{tot} cross sections are listed. First, we note the significant role that the breakup channel plays in the $^{11}\text{Li}+p$ reaction, where σ_{bu}^{tot} contributes more than 80% to σ_R^{tot} . This is not the case of $^6\text{He}+^{12}\text{C}$ process at energy of 38.3 MeV/nucleon [54], for which the breakup cross section constitutes only about the half of the total reaction cross section. This can be related with the observation that a quite substantial amount of the $^{11}\text{Li}+p$ imaginary potential in the elastic scattering channel is formed due to a transfer of the incident flux of ^{11}Li to a larger extent into breakup chan-

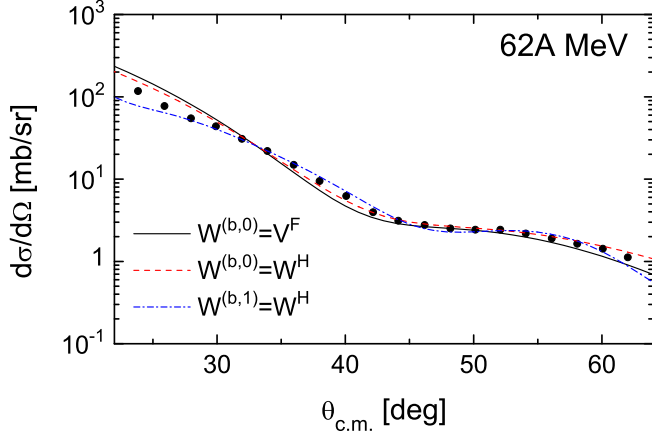


FIG. 9. (Color online) The $^{11}\text{Li}+p$ elastic scattering cross section at $E = 62$ MeV/nucleon using $U^{(b,n)}$ [Eq. (16)] for values of the parameters N shown in Table III. Black solid line: $W^{(b,0)} = V^F$, red dashed line: $W^{(b,0)} = W^H$, and blue dash-dotted line: $W^{(b,1)} = W^H$. The experimental data are taken from Ref. [21].

TABLE III. The N 's parameters of OP's for $^{11}\text{Li}+p$ scattering at 62 MeV/nucleon and HEA estimations of the total cross sections σ_{abs}^{tot} [Eq. (20)], σ_{bu}^{tot} [Eq. (23)], and σ_R^{tot} [Eq. (24)] (in mb) using the cluster model of ^{11}Li .

$W^{(b,n)}$	N_R	N_I	σ_{abs}^{tot}	σ_{bu}^{tot}	σ_R^{tot}
$W^{(b,0)} = V^F$	1.407	1.195	79.0	431.8	510.8
$W^{(b,0)} = W^H$	1.381	1.306	78.6	405.3	483.9
$W^{(b,1)} = W^H$	4.68	3.99	106.6	581.6	688.2

nels. Also, for the case of $n = 1$ state of the cluster wave function, the fitted strength coefficients N 's and the respective values of the cross sections are larger than for the $n = 0$ state, but the general conclusions on the preferable role of breakup processes remain the same.

Our next step is to calculate using Eqs. (28) and (29) as examples the cross sections of the diffractive and stripping (when $h = 2n$ cluster leaves the elastic channel) $^{11}\text{Li}+p$ reactions at $E = 62$ MeV/nucleon, respectively. For this purpose we use in Eqs. (28) and (29) the corresponding functions $S_i(b_i)$, $i = c, h$ [see Eq. (19)]. They are given in Fig. 10 for s -state with $n=0$ and $n=1$. In Figs. 11 and 12 we show the results for the diffraction breakup and stripping $^{11}\text{Li}+p$ scattering at $E = 62$ MeV/nucleon, respectively. These results give predictions because of missing experimental data for such processes accompanying the $^{11}\text{Li}+p$ scattering at $E \leq 100$ MeV/nucleon. For the diffractive scattering we obtain values of the widths 98 MeV/c (for $n=0$) and 85 MeV/c (for $n=1$) and for the stripping reaction 79 MeV/c (for $n=0$) and 72 MeV/c (for $n=1$), respectively, thus favoring the configuration in which the two valence neutrons

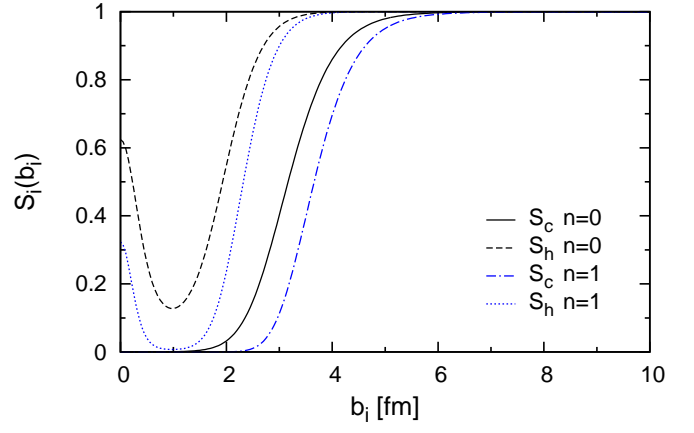


FIG. 10. (Color online) The functions $S_i(b_i)$, $i = c, h$ [see Eq. (19)] for s -state of the relative motion of clusters with $n=0$ and $n=1$.

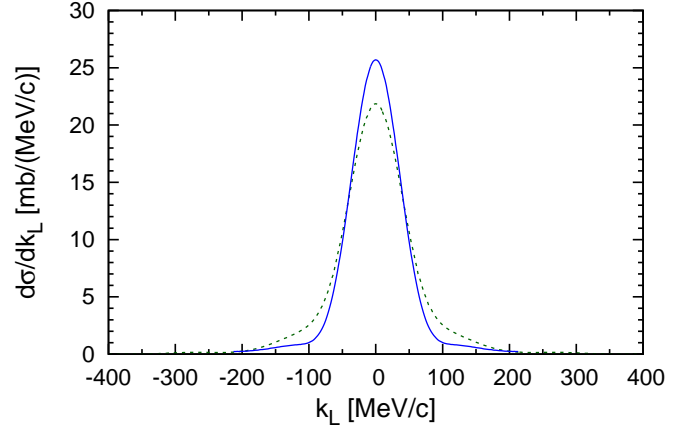


FIG. 11. (Color online) Cross section of diffraction breakup in $^{11}\text{Li}+p$ scattering at $E = 62$ MeV/nucleon for the cases of $n=0$ (green dashed line) and $n=1$ (blue solid line).

occupy $1s$ state in ^{11}Li . It is worth to be noted that the calculated in our work widths for the ^{11}Li breakup on the proton target are larger than those obtained in the experiments (around 50 MeV/c) for the reactions of ^{11}Li on the nuclear targets ^9Be , ^{93}Nb and ^{181}Ta at energy 66 MeV/nucleon [11] and on a wide range of targets (^9Be to ^{238}U) [12]. It is noted in [11, 12] that the width almost does not depend on the target's mass number and thus, it characterizes basically the momentum distribution of two clusters. Our width for the stripping of $2n$ -cluster is similar to the cases of $2n$ stripping from other nuclei (but not from ^{11}Li). It turns out that the account for the $2n$ binding in ^{11}Li is not enough to obtain the observed widths in the scattering of ^{11}Li on nuclei, as well as on proton targets. We would like to mention also that we had a methodical task to calculate the widths using different wave functions ($n = 0, 1$) of the relative motion of the clusters. The results show similar values of the widths in both cases. Probably, it is difficult to solve the problem within our simplified two-cluster model

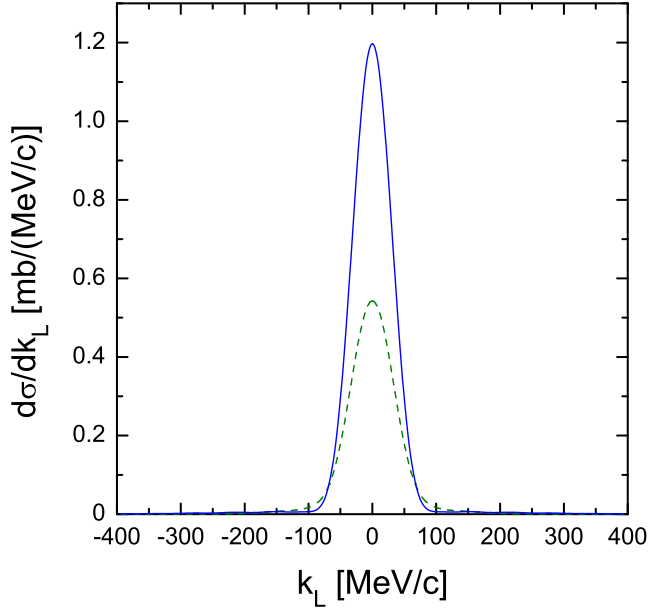


FIG. 12. (Color online) The same as in Fig. 11 but for the stripping reaction.

and thus, it must be considered in a more complicated three-body model. Also, obviously experiments on stripping and diffraction reactions of ^{11}Li on proton targets are highly desirable. This concerns measurements of the neutrons in the decay, as well.

D. Single-particle density of ^{11}Li in two-cluster model

In this subsection we would like to consider in more details the single-particle density distribution of ^{11}Li , which can be calculated and applied instead of phenomenological one in the analyses and interpretation of $^{11}\text{Li}+p$ experimental data. For this purpose, we adopt our cluster model, consisting of ^9Li core and halo $h = 2n$. If one sets $\rho_h(\mathbf{r}_1)$ for the h -cluster and $\rho_c(\mathbf{r}_2)$ for ^9Li nucleus, then the single-particle density distribution of ^{11}Li can be derived in analogy to Eq. (16) in the following form:

$$\rho(r) = \int d\phi \sin\theta d\theta \int ds s^2 [\rho_h(\mathbf{r}_h) + \rho_c(\mathbf{r}_c)] \rho_0^{(n)}(\mathbf{s}) = 2\pi \int_{-1}^1 dx \times \int_0^\infty ds s^2 \left[\rho_h \left(\sqrt{r^2 - 2(9/11)rsx + (9/11)^2s^2} \right) + \rho_c \left(\sqrt{r^2 + 2(2/11)rsx + (2/11)^2s^2} \right) \right] \rho_0^{(n)}(\mathbf{s}). \quad (30)$$

The expression (30) indicates that the density of ^{11}Li can be calculated using the sum of the corresponding densities of both clusters and folding it with the square of the relative-motion wave function of the two clusters $|\phi_{00}(\mathbf{s})|^2$.

As a comment of our approach we would like to mention the difference between the method to calculate the folding $^{11}\text{Li}+p$ OP [Eq. (16)] and that to estimate the single-particle density of ^{11}Li [Eq. (30)]. In fact, in the former, the U_h optical potential was not calculated as a folding integral, but expressed through the v_{np} potentials, and therefore there we did not include the density of the $h = 2n$ cluster. Instead, in Eq. (30) we consider the h -cluster density, together with the density of the ^9Li core, both being folded by the wave function of the relative motion of the two clusters.

Further, in the calculations we use the LSSM density for the ^9Li cluster with rms radius $R_c=2.31$ fm [43] and for the h -halo we probe two densities: the one being described by the Gaussian function (G density) (e.g., [61])

$$\rho^G(r) = \left(\frac{3}{2\pi R_h^2} \right)^{3/2} \exp\left(-\frac{3r^2}{2R_h^2} \right) \quad (31)$$

and the other one is the symmetrized Fermi distribution (SF density) (e.g., [62])

$$\rho^{SF}(r) = \rho_0 \frac{\sinh(R/a)}{\cosh(R/a) + \cosh(r/a)}, \quad (32)$$

where

$$\rho_0 = \frac{3}{4\pi R^3} \left[1 + \left(\frac{\pi a}{R} \right)^2 \right]^{-1} \quad (33)$$

and the corresponding rms radius is:

$$\langle r^2 \rangle = R_h^2 = \frac{3}{5} R^2 \left[1 + \frac{7}{3} \left(\frac{\pi a}{R} \right)^2 \right]. \quad (34)$$

The two densities [Eqs. (31) and (32)] are normalized to unity and substituting them in Eq. (30) they have to be multiplied by a factor of 2. As for the G density it has only one parameter, the rms radius of the halo R_h , that governs its behavior. First, we take $R_h=2$ fm which is almost twice the nucleon radius. In principle, such a choice of R_h is justified since the cluster inside the nucleus is "smeared" and, moreover, the folding procedure itself (in which the relative motion function $\phi_{00}(\mathbf{s})$ takes place with rms radius 4.93 fm, see also Sec. III.A) ensures

TABLE IV. Values of the parameters of the symmetrized Fermi and Gaussian density distributions, h - and c -cluster rms radii R_h and R_c , and deduced matter rms radii R_m (in fm) within the ${}^9\text{Li}+2n$ model of ${}^{11}\text{Li}$.

Parametrization	R	a	R_h	R_c	R_m
SF1	2.234	0.27	2	2.31 ^a	2.77 ($n=0$) 2.93 ($n=1$)
G			2	2.31 ^a	2.77 ($n=0$) 2.93 ($n=1$)
SF2	4.573	0.5	4	2.31 ^a	3.32 ($n=1$)
0.2GG+0.8GO [20]			5.98	2.52	3.42

^a From LSSM for ${}^9\text{Li}$

the h -cluster to be in the periphery. Concerning the SF density, we perform calculations with a set of parameters R and a , selected so that to obey rms $R_h=2$ fm (see the set SF1 in Table IV). For the choice of them the condition $R > \pi a$ must be satisfied and for a more convenience Eq. (34) can be rewritten in the following way:

$$R^2 = \frac{5}{3}R_h^2 - \frac{7}{3}(\pi a)^2. \quad (35)$$

The calculated single-particle density distributions of ${}^{11}\text{Li}$ are presented in Fig. 13 together with the LSSM density. Results are shown for both $n=0$ and $n=1$ cases. As can be seen, the usage of two kinds of h -density SF1 and G yields very similar ${}^{11}\text{Li}$ densities shown as the pair of the dotted and dashed curves for $n=0$, and also as the solid and dot-dashed curves for $n=1$, correspondingly, in the whole region of r up to 10 fm. In addition, all these four curves are close at $r < 4$ fm. However, the difference between the $n=0$ and $n=1$ pairs is seen in the interval $5 < r < 7$ fm, where the $n=1$ curves exhibit a "bump", while the $n=0$ ones go down as compared to the case of the LSSM density of ${}^{11}\text{Li}$. Moreover, we note that the ${}^{11}\text{Li}$ rms radius of 2.93 fm for $n=1$ curves is very close to the LSSM value of 2.94 fm. The tail of the LSSM density is higher at $r > 8$ fm than those of the cluster curves with $R_h = 2$ fm, but as it was pointed out in Ref. [20] the calculated differential cross sections of ${}^{11}\text{Li}+p$ scattering are not sensitive to a possible long density tail at the nuclear far periphery.

The very pronounced halo nature of ${}^{11}\text{Li}$ nucleus is mainly supported by its large matter radius exhibited by Tanihata *et al.* in Ref. [1]. Recently, a successful attempt to get a "realistic" density of this nucleus was realized in Ref. [20]. In the latter the experimental data at about 700 MeV/nucleon were described using the phenomenological constituent cluster model of the ${}^{11}\text{Li}$ density composed of two terms 0.2GG+0.8GO with the Gaussian GG and the harmonic oscillator GO functions together. The fitting procedure led to the total rms matter radius $R_m = 3.42$ fm of the whole density, where the fitted values $R_c = 2.52$ fm and $R_h = 5.98$ fm of its separate terms were inter-

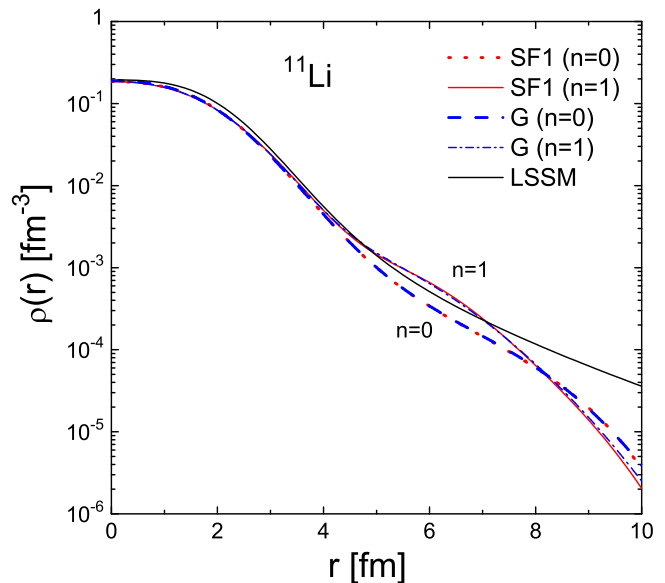


FIG. 13. (Color online) Single-particle density distribution of ${}^{11}\text{Li}$ (normalized to $A = 11$) obtained in the framework of the cluster model [Eq. (30)]. The h -cluster density distributions are taken in two forms: symmetrized Fermi distribution (SF1) and Gaussian function (G) with $R_h = 2$ fm. The results are presented for the cases of $n=0$ and $n=1$, respectively. The LSSM density is also given.

preted as the core and h -halo radii, respectively. These radii satisfy the relation

$$R_m^2 = \frac{A_c R_c^2 + A_h R_h^2}{A}, \quad A = A_c + A_h, \quad (36)$$

(A_c , A_h , and A being number of nucleons in the core, in the $2n$ -cluster and the nucleus, respectively) that is valid for the constituent model. However, instead we may argue that the ${}^9\text{Li}$ and h -systems can be considered as the true clusters only when in a cluster model they are folded [see Eq. (30)] with the probability density of their relative motion. In Fig. 14 our result is shown as the SF2 curve when the value of $R_h = 4$ fm is taken to be twice larger than $R_h = 2$ fm in the SF1 case. Also in the same figure we present the phenomenological 0.2GG+0.8GO density from Ref. [20]. Our SF2 parametrization leads to a value for the matter rms radius $R_m = 3.32$ fm that is close to $R_m = 3.42$ fm for the phenomenological constituent model mentioned above. Thus, our folding method to calculate the single-particle density distribution [Eq. (30)] which takes into account the relative motion of the clusters makes it possible to get realistic densities within cluster models without use of phenomenology. It is seen from our analysis with SF2 parametrization that the h -cluster is really "smeared" in ${}^{11}\text{Li}$ nucleus ($R_h = 4$ fm) and that the averaging on a relative motion of both clusters (which strongly depends on the h -cluster separation energy) plays an important role. This fact is confirmed also in Ref. [20], where the deduced halo radius $R_h = 5.98$ fm is larger than the core radius $R_c = 2.52$ fm by a factor

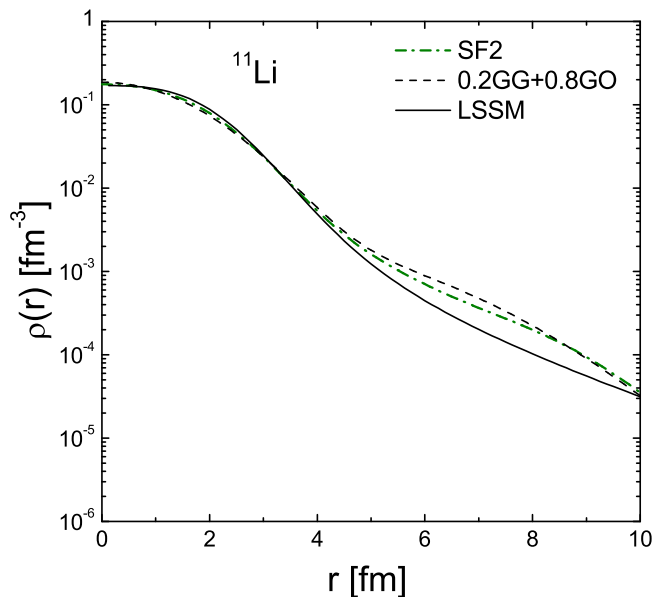


FIG. 14. (Color online) Single-particle density distribution of ^{11}Li (normalized to $A = 11$) obtained in the framework of the cluster model [Eq. (30)] with symmetrized Fermi (SF2) distribution for the h -cluster density with $R_h = 4$ fm (green dash-dotted line). The black dashed line represents the best density parametrization that describes the $^{11}\text{Li}+p$ elastic scattering data [20], while the black solid line is the LSSM density.

of more than 2. However, the ambiguity remains in the choice of the "best" density distribution of ^{11}Li because only the $^{11}\text{Li}+p$ elastic scattering data are not sufficient.

IV. CONCLUSIONS

The results of the present work can be summarized as follows:

(i) In the first part of the work (Sec. II) the microscopic optical potentials and cross sections of $^{11}\text{Li}+p$ elastic scattering were calculated at the energies of 62, 68.4, and 75 MeV/nucleon and were compared with the available experimental data. The direct (V^D) and exchange (V^{EX}) parts of the real OP (V^F) were calculated using the folding procedure with density-dependent M3Y (CDM3Y6-type) effective interaction based on the Paris NN potential. The imaginary part of OP (W^H) was calculated microscopically within the folding model based on the high-energy approximation. The LSSM densities [43] of protons and neutrons with exponential asymptotic behavior of ^{11}Li that is the correct one were used in the calculations. The spin-orbit contribution to the OP was also included in the calculations. The $^{11}\text{Li}+p$ elastic scattering cross sections and the total reaction cross sections were calculated using the program DWUCK4 [48].

(ii) We pointed out that the regularization of our microscopic OP's is achieved by introducing the fitting pa-

rameters N_R , N_I , N_R^{SO} , N_I^{SO} related to the "depths" of the separate parts of OP. They are, in principle, the only free parameters of our approach, in contrast to other phenomenological ones and serve as a quantitative test of the latter, i.e. the proximity of N 's values to unity shows the closeness of the approach to the reality. However, here the "ill-posed" problem takes place because the fitting procedure is applied to a limited number of experimental data. The problem of the ambiguity of the N 's parameters have been considered in our previous works [45, 46]. We used in the present work a physical constraint on the choice of the values of the N 's parameters, namely the known behavior of the volume integrals J_V and J_W as functions of the incident energy for $E \leq 100$ MeV/nucleon [53]. We compare the behavior of the values of J_V and J_W obtained in our work with those in the semi-phenomenological approach in Ref. [37], where much more parameters have been used than in our microscopic method. We discuss in more details the problem arising from the behavior of J_W at $E = 62$ MeV/nucleon and relate it to the quality of the data at larger angles ($\theta_{c.m.} > 46^\circ$). We note that this problem had appeared also in [37]. Finally, we obtained a definite set of the fitted N 's parameters that give satisfactory agreement of our results with the data of elastic $^{11}\text{Li}+p$ scattering cross section using the physical criterion of the behavior of the volume integrals as functions of the energy.

(iii) We would like to mention that the values of the total cross sections of scattering and reaction can serve as another physical criterion for the N 's values. However, the corresponding experimental data for these values are missing at the energy interval considered in our work, so they are highly desirable.

(iv) As in our previous works [45, 46], we would like to emphasize that a more successful explanation of the cross section data could be given by accounting for virtual excitations of inelastic and decay channels of the reaction. For this reason, in Sec. III of the present paper, apart from the usual folding model based on the LSSM, we consider another folding approach that includes ^{11}Li breakup suggesting a simple $^9\text{Li}+2n$ cluster model for its structure. Both LSSM and cluster models of ^{11}Li are capable to reproduce fairly well the two-neutron separation energy from ^{11}Li . In Sec. III we use the procedure from the first part of our work (Sec. II) for microscopic calculations of the necessary OP's in the breakup model for estimations of the elastic scattering cross sections, as well as of the momentum distributions in the processes of the proton scattering on clusters and the corresponding S -functions in $^9\text{Li}+p$ and $h+p$ scattering. The folding OP's calculated in the two parts of our work behave rather closely if one fits their strengths to the same elastic scattering data, as it is done for $^{11}\text{Li}+p$ at energy 62 MeV/nucleon. Thus, the analysis of other types of the reaction mechanism, such as the ^{11}Li breakup, makes it possible to understand their significant role in the formation of the OP responsible for the $^{11}\text{Li}+p$ elastic scattering. It turns out that the breakup channel gives σ_{bu}^{tot} that

exceeds 80% from σ_R^{tot} , while it is around a half of σ_R^{tot} in the case of ${}^6\text{He}+{}^{12}\text{C}$ (as obtained in Ref. [54]).

(v) In the present work we give also predictions for the longitudinal momentum distributions of ${}^9\text{Li}$ fragments produced in the breakup of ${}^{11}\text{Li}$ at 62 MeV/nucleon on a proton target. We calculated the diffraction and stripping (when the cluster $2n$ leaves the elastic channel) cross sections of the reaction of ${}^{11}\text{Li}$ on proton target at energy 62 MeV/nucleon. We note that our breakup gives the width of the peak between 70 and 80 MeV/c, while the widths of about 50 MeV/c are known from the reactions of ${}^{11}\text{Li}$ on nuclear targets ${}^9\text{Be}$, ${}^{93}\text{Nb}$ and ${}^{181}\text{Ta}$ at energy 66 MeV/nucleon. In relation with this, here we should mention that at the energy of the range 60-70 MeV/nucleon a distortion due to the nuclear and Coulomb forces could affect the cross sections. We have in mind also that our simplified two-cluster model could not give the correct answer and that it can be found in a more complicated three-body approach. Hence, this problem remains open and requires further analysis. We emphasize the necessity of experiments on stripping and diffraction reactions of ${}^{11}\text{Li}$ on proton targets at energy $E < 100$ MeV/nucleon.

(vi) We present results for the single-particle density distribution of ${}^{11}\text{Li}$ in the framework of a cluster model. Our calculated density is close to the phenomenological one obtained in Ref. [20] by fitting to the experimental differential cross sections of scattering of ${}^{11}\text{Li}$ at 700

MeV/nucleon on a proton target. From a physical point of view the cluster model allows more clear interpretation of the experimental data and together with the phenomenological densities can be applied as a pattern density to fit the data. Future measurements of the cross sections for proton elastic scattering and momentum distribution of the ${}^9\text{Li}$ fragments in the ${}^{11}\text{Li}$ breakup reactions might provide supplemental information on the internal spatial structure of the ${}^{11}\text{Li}$ nucleus.

ACKNOWLEDGMENTS

The authors are grateful to Professor N.S. Zelenskaya and Professor S.N. Ershov for helpful discussions. The work is partly supported by the Project from the Agreement for co-operation between the INRNE-BAS (Sofia) and JINR (Dubna). Four of the authors (D.N.K., A.N.A., M.K.G. and K.S.) are grateful for the support of the Bulgarian Science Fund under Contract No. 02-285 and one of them (D.N.K.) under Contract No. DID-02/16-17.12.2009. The authors E.V.Z. and K.V.L. thank the Russian Foundation for Basic Research (Grants Nos. 12-01-00396 and 13-01-00060) for partial support. K.S. acknowledges the support of the Project BG-051P0001-3306-003.

-
- [1] I. Tanihata, H. Hamagaki, O. Hashimoto, S. Nagamiya, Y. Shida, N. Yoshikawa, O. Yamakawa, K. Sugimoto, T. Kobayashi, D. E. Greiner, N. Takahashi, and Y. Nojiri, *Phys. Lett. B* **160**, 380 (1985).
- [2] I. Tanihata, H. Hamagaki, O. Hashimoto, Y. Shida, N. Yoshikawa, K. Sugimoto, O. Yamakawa, T. Kobayashi, and N. Takahashi, *Phys. Rev. Lett.* **55**, 2676 (1985).
- [3] I. Tanihata, T. Kobayashi, O. Yamakawa, T. Shimoura, K. Ekuni, K. Sugimoto, N. Takahashi, T. Shimoda, and H. Sato, *Phys. Lett. B* **206**, 592 (1988).
- [4] W. Mittig, J. M. Chouvel, Z. W. Long, L. Bianchi, A. Cunsolo, B. Fernandez, A. Foti, J. Gastebois, A. Gillibert, C. Gregoire, Y. Schutz, and C. Stephan, *Phys. Rev. Lett.* **59**, 1889 (1987).
- [5] P. G. Hansen and B. Jonson, *Eur. Lett.* **4**, 409 (1987).
- [6] A. B. Migdal, *Sov. J. Nucl. Phys.* **16**, 238 (1973).
- [7] T. Kobayashi *et al.*, *Phys. Rev. Lett.* **60**, 2599 (1988).
- [8] G. F. Bertsch, B. A. Brown, and H. Sagawa, *Phys. Rev. C* **39**, 1154 (1989); T. Hoshino, H. Sagawa, and A. Arima, *Nucl. Phys. A* **506**, 271 (1990); L. Johannsen, A. S. Jensen, and P. G. Hansen, *Phys. Lett. B* **244**, 357 (1990); A. C. Hayes, *ibid* **254**, 15 (1991); G. F. Bertsch and H. Esbensen, *Ann. Phys.* **209**, 327 (1991); Y. Tosaka and Y. Suzuki, *Nucl. Phys. A* **512**, 46 (1990).
- [9] R. Anne *et al.*, *Phys. Lett. B* **250**, 19 (1990).
- [10] H. Esbensen, *Phys. Rev. C* **44**, 440 (1991); *ibid.* **53**, 2007 (1996).
- [11] N. A. Orr, N. Anantaraman, Sam M. Austin, C.A. Bertulani, K. Hanold, J. H. Kelley, D. J. Morrissey, B. M. Sherrill, G. A. Souliotis, M. Thoennessen, J. S. Winfield and J. A. Winger, *Phys. Rev. Lett.* **69**, 2050 (1992).
- [12] N. A. Orr, N. Anantaraman, Sam M. Austin, C.A. Bertulani, K. Hanold, J. H. Kelley, R. A. Kryger, D. J. Morrissey, B. M. Sherrill, G. A. Souliotis, M. Steiner, M. Thoennessen, J. S. Winfield, J. A. Winger, and B. M. Young, *Phys. Rev. C* **51**, 3116 (1995).
- [13] D. Baye and P. Capel, *Lecture Notes in Physics*, vol. 848, pp.121-163 (2012).
- [14] F. Barranco, E. Vigezzi, and R. A. Broglia, *Z. Phys. A* **356**, 45 (1996).
- [15] K. Hencken, G. Bertsch, and H. Esbensen, *Phys. Rev. C* **54**, 3043 (1996).
- [16] C. A. Bertulani and P. G. Hansen, *Phys. Rev. C* **70**, 034609 (2004).
- [17] C. A. Bertulani and K. W. McVoy, *Phys. Rev. C* **46**, 2638 (1992).
- [18] S. N. Ershov, B. V. Danilin, J. S. Vaagen, A. A. Korshennikov, and I. J. Thompson, *Phys. Rev. C* **70**, 054608 (2004).
- [19] C. A. Bertulani, M. Hussein, and G. Muenzenberg, *Physics of Radioactive Beams* (Nova Science, Hauppauge, New York, 2002), ISBN: 1-59033-141-9.
- [20] A. V. Dobrovolsky, G. D. Alkhalov, M. N. Andronenko, A. Bauchet, P. Egelhof, S. Fritz, H. Geissel, C. Gross, A. V. Khanzadeev, G. A. Korolev, G. Kraus, A. A. Lobodenko, G. Muenzenberg, M. Mutterer, S. R. Neumaier, T. Schäfer, C. Scheidenberger, D. M. Seliverstov, N. A. Timofeev, A. A. Vorobyov, and V. I. Yatsoura, *Nucl. Phys.*

- A **766**, 1 (2006).
- [21] C.-B. Moon, M. Fujimaki, S. Hirenzaki, N. Inabe, K. Katori, J. C. Kim, Y. K. Kim, T. Kobayashi, T. Kubo, H. Kumagai, S. Shimoura, T. Suzuki, and I. Tanihata, Phys. Lett. B **297**, 39 (1992).
- [22] A. A. Korshennikov, E. A. Kuzmin, E. Yu. Nikolskii, O. V. Bochkarev, S. Fukuda, S. A. Goncharov, S. Ito, T. Kobayashi, S. Momota, B. G. Novatskii, A. A. Ogloblin, A. Ozawa, V. Pribora, I. Tanihata, and K. Yoshida, Phys. Rev. Lett. **78**, 2317 (1997).
- [23] A. A. Korshennikov, E. Yu. Nikolskii, T. Kobayashi, A. Ozawa, S. Fukuda, E. A. Kuzmin, S. Momota, B. G. Novatskii, A. A. Ogloblin, V. Pribora, I. Tanihata, and K. Yoshida, Phys. Rev. C **53**, R537 (1996).
- [24] M. V. Zhukov, B. V. Danilin, D. V. Fedorov, J. M. Bang, I. J. Thompson, and J. S. Vaagen, Phys. Rep. **231**, 151 (1993).
- [25] Y. Suzuki, K. Yabana, and Y. Ogawa, Phys. Rev. C **47**, 1317 (1993).
- [26] M. Kohno, Phys. Rev. C **48**, 3122 (1993).
- [27] A. K. Chaudhuri, Phys. Rev. C **49**, 1603 (1994).
- [28] R. Kanungo and C. Samanta, Nucl. Phys. A **617**, 265 (1997).
- [29] Y. J. Kim and M. H. Cha, Int. J. Mod. Phys. E **10**, 91 (2001).
- [30] R. Crespo, J. A. Tostevin, and I. J. Thompson, Phys. Rev. C **54**, 1867 (1996).
- [31] K. Amos, W. A. Richter, S. Karataglidis, and B. A. Brown, Phys. Rev. Lett. **96**, 032503 (2006); P. K. Deb, B. C. Clark, S. Hama, K. Amos, S. Karataglidis, and E. D. Cooper, Phys. Rev. C **72**, 014608 (2005).
- [32] M. Avrigeanu, G. S. Anagnostatos, A. N. Antonov, and J. Giapitzakis, Phys. Rev. C **62**, 017001 (2000); M. Avrigeanu, G. S. Anagnostatos, A. N. Antonov, and V. Avrigeanu, Int. J. Mod. Phys. E **11**, 249 (2002); M. Avrigeanu, A. N. Antonov, H. Lenske, and I. Stetcu, Nucl. Phys. A **693**, 616 (2001).
- [33] G. R. Satchler and W. G. Love, Phys. Rep. **55**, 183 (1979); G. R. Satchler, *Direct Nuclear Reactions* (Clarendon, Oxford, 1983).
- [34] D. T. Khoa and W. von Oertzen, Phys. Lett. B **304**, 8 (1993); **342**, 6 (1995); D. T. Khoa, W. von Oertzen, and H. G. Bohlen, Phys. Rev. C **49**, 1652 (1994); D. T. Khoa, W. von Oertzen and A. A. Ogloblin, Nucl. Phys. A **602**, 98 (1996); Dao T. Khoa and Hoang Sy Than, Phys. Rev. C **71**, 014601 (2005); O. M. Knyaz'kov, Sov. J. Part. Nucl. **17**, 137 (1986).
- [35] D. T. Khoa and G. R. Satchler, Nucl. Phys. A **668**, 3 (2000).
- [36] D. T. Khoa, G. R. Satchler, and W. von Oertzen, Phys. Rev. C **56**, 954 (1997).
- [37] M. Y. M. Hassan, M. Y. H. Farag, E. H. Esmael, and H. M. Maridi, Phys. Rev. C **79**, 014612 (2009).
- [38] M. Y. H. Farag, E. H. Esmael, and H. M. Maridi, Eur. Phys. J. A **48**, 154 (2012).
- [39] K. V. Lukyanov, E. V. Zemlyanaya, and V. K. Lukyanov, JINR Preprint P4-2004-115, Dubna, 2004; Phys. At. Nucl. **69**, 240 (2006).
- [40] P. Shukla, Phys. Rev. C **67**, 054607 (2003).
- [41] R. J. Glauber, *Lectures in Theoretical Physics* (New York, Interscience, 1959), p.315.
- [42] A. G. Sitenko, Ukr. Fiz. J. **4**, 152 (1959).
- [43] S. Karataglidis, P. G. Hansen, B. A. Brown, K. Amos, and P. J. Dortmans, Phys. Rev. Lett. **79**, 1447 (1997); S. Karataglidis, P. J. Dortmans, K. Amos, and C. Bennhold, Phys. Rev. C **61**, 024319 (2000).
- [44] K. V. Lukyanov, V. K. Lukyanov, E. V. Zemlyanaya, A. N. Antonov, and M. K. Gaidarov, Eur. Phys. J. A **33**, 389 (2007).
- [45] V. K. Lukyanov, E. V. Zemlyanaya, K. V. Lukyanov, D. N. Kadrev, A. N. Antonov, M. K. Gaidarov, and S. E. Massen, Phys. Rev. C **80**, 024609 (2009).
- [46] V. K. Lukyanov, D. N. Kadrev, E. V. Zemlyanaya, A. N. Antonov, K. V. Lukyanov, and M. K. Gaidarov, Phys. Rev. C **82**, 024604 (2010).
- [47] V. K. Lukyanov, D. N. Kadrev, E. V. Zemlyanaya, A. N. Antonov, K. V. Lukyanov, M. K. Gaidarov, and K. Spasova, Phys. At. Nucl. **75**, 1407 (2012).
- [48] P. D. Kunz and E. Rost, in *Computational Nuclear Physics*, edited by K. Langanke *et al.* (Springer-Verlag, New York, 1993), Vol.2, p.88.
- [49] P. Shukla, arXiv: nucl-th/0112039.
- [50] S. Charagi and G. Gupta, Phys. Rev. C **41**, 1610 (1990); **46**, 1982 (1992).
- [51] C. Xiangzhou, F. Jun, S. Wenqing, M. Yugang, W. Jiansong, and Y. Wei, Phys. Rev. C **58**, 572 (1998).
- [52] A. N. Tikhonov and V. Y. Arsenin, *Solutions of Ill-Posed Problems*, (V. H. Winston and Sons, Wiley, New York, 1977).
- [53] E. A. Romanovsky *et al.*, Bulletin of the Russian Academy of Sciences: Physics **62**, No.1, 150 (1998).
- [54] V. K. Lukyanov, E. V. Zemlyanaya, and K. V. Lukyanov, Int. J. Mod. Phys. E **20**, 2039 (2011).
- [55] I. J. Thompson and M. V. Zhukov, Phys. Rev. C **49**, 1904 (1994).
- [56] L. I. Galanina and N. S. Zelenskaya, Bulletin of the Russian Academy of Sciences: Physics **77**, No.4, 383 (2013); Phys. At. Nucl. **76**, No.12 (2013), in print.
- [57] T. Myo, K. Kato, H. Toki, and K. Ikeda, Phys. Rev. C **76**, 024305 (2007).
- [58] J. A. Tostevin, R. C. Johnson, and J. S. Al-Khalili, Nucl. Phys. A **630**, 340c (1998).
- [59] S. N. Ershov, L. V. Grigorenko, J. S. Vaagen, and M. V. Zhukov, J. Phys. G **37**, 064026 (2010).
- [60] D. R. Thompson, M. LeMere, and Y. C. Tang, Nucl. Phys. A **286**, 53 (1977); Y. C. Tang, M. LeMere, and D. R. Thompson, Phys. Rep. **47**, 167 (1978).
- [61] G. D. Alkhasov, A. V. Dobrovolsky, P. Egelhof, H. Geissel, H. Irnich, A. V. Khanzadeev, G. A. Korolev, A. A. Lobodenko, G. Mützenber, M. Mutterer, S. R. Neumaier, W. Schwab, D. M. Seliverstov, T. Suzuki, and A. A. Vorobyov, Nucl. Phys. A **712**, 269 (2002).
- [62] V. V. Burov and V. K. Lukyanov, Preprint JINR, R4-11098, 1977, Dubna; V. V. Burov, D. N. Kadrev, V. K. Lukyanov, and Yu. S. Pol', Phys. At. Nuclei **61**, 525 (1998).